ACKNOWLEDGMENTS

The authors wish to express their appreciation for the hospitality of the Department of Physics, University of North Carolina (U.N.C.), where the measurements were performed partly under the support of the Advanced Research Projects Agency. We would like to acknowledge the stimulating discussions concerning the theory with D. Fraitova; thanks are also due to C. Ross from the Computation Center, U.N.C., for a valuable suggestion in the solution of the Eqs. (16). C. V. Briscoe and E. N. Mitchell from the Department of Physics, U.N.C., and D. S. Rodbell from the General Electric Research Laboratories made helpful comments concerning the measurements and the manuscript. Further, we are greatly indebted to B. Sestak and Z. Tahal for growing the single crystals and to J. Caslavsky, B. Heinrich, J. Hejduk and M. Simanova, all from the Institute of Physics, Prague, Czechoslovakia, for help with the sample preparation.

PHYSICAL REVIEW VOLUME 139, NUMBER 4A 16 AUGUST 1965

Fermi Surfaces of Cr, Mo, and W by the Augmented-Plane-Wave Method*

T. L. Loucks

Institute for Atomic Research and Department of Physics, Iowa State University, Ames, Iowa

(Received 16 March 1965)

The Fermi surfaces of chromium, molybdenum, and tungsten were calculated using linear-variation functions consisting of 19 augmented plane waves (APW). The muffin-tin potential was constructed from a superposition of atomic potentials centered on the lattice sites. The atomic orbitals were solutions of the Hartree-Fock-Slater self-consistent field. Constant-energy surfaces throughout the Brillouin zone and the volume contained by each of the regions were determined. The Fermi surface was selected from these energy surfaces by the requirement of equal hole and electron volumes. The density of states at the Fermi energy was determined from the slope of the volume-vs-energy curve. The Fermi surfaces of Mo and W were found to be almost identical and similar to the model postulated by Lomer for the Cr-group metals. The Fermi surface of Cr, however, differs from the other two by the disappearance of the hole pockets around N and a shrinking of the knobs on the electron jack. A quantitative comparison between experimental results and the Fermi surface of Mo is presented.

I. INTRODUCTION

A MODEL for the Fermi surface of the chromium-group metals was proposed in 1962 by Lomer.[1] This model was not the result of *ab initio* electronic-structure calculations for these elements. It was deduced from the energy bands for iron which had been determined theoretically by Wood[2] using the augmented-plane-wave (APW) method. Also available for consideration at that time was a tight-binding calculation for Cr by Asdente and Friedel[3] in which only the d bands were considered. Prior to this, there was work done on W by Manning and Chodorow[4] using the cellular method.

The Lomer model has met with varying degrees of success in comparisons with experimental results. In the original paper the larger pieces of the surface (holes at H, electrons at Γ) were discussed qualitatively, and the antiferromagnetic state of Cr was considered. In a brief note two years later, Lomer[5] corrected the model such that it was consistent with the requirements imposed by crystal symmetry. Here again the qualitative features of the larger pieces of the surface were discussed.

In 1963 Brandt and Rayne[6] reported de Haas–van Alphen data for the three metals. However, these frequencies corresponded to very small pieces of the surface not well defined in the model (holes at N and either electrons or hole pockets along ΓH). Nevertheless, it was observed that the results for Mo and W were quite similar to each other and different from those for Cr. Further low-field measurements on W by Sparlin and Marcus[7,8] have been interpreted by these authors as suggesting that the electron surface at Γ has the shape of a child's jack with knobs at the end of each arm. Additional de Haas–van Alphen data for W has been reported by Girvan,[9] which lends further support to the general features of the larger pieces of the Lomer model. The size-effect experiments by Walsh[10] have pointed out the separation of the electron and hole regions along ΓH, attributed to spin-orbit coupling.

* Contribution No. 1674. Work was performed in the Ames Laboratory of the U. S. Atomic Energy Commission.

[1] W. M. Lomer, Proc. Phys. Soc. (London) **80**, 489 (1962).
[2] J. H. Wood, Phys. Rev. **126**, 517 (1962).
[3] M. Asdente and J. Friedel, Phys. Rev. **124**, 384 (1961).
[4] M. F. Manning and M. I. Chodorow, Phys. Rev. **56**, 787 (1939)
[5] W. M. Lomer, Proc. Phys. Soc. (London) **84**, 327 (1964).
[6] G. B. Brandt and J. A. Rayne, Phys. Rev. **132**, 1945 (1963).
[7] D. M. Sparlin and J. A. Marcus, Bull. Am. Phys. Soc. **8**, 258 (1963).
[8] D. M. Sparlin and J. A. Marcus, Bull. Am. Phys. Soc. **9**, 250 (1964).
[9] R. F. Girvan, M.S. thesis, Iowa State University, 1964 (unpublished).
[10] W. M. Walsh, Jr., and C. C. Grimes, Phys. Rev. Letters **13**, 523 (1964).

In light of the general qualitative success of this model, it was decided to perform *ab initio* calculations of the Fermi surfaces for the chromium group, in the hope of obtaining quantitative information which could be compared with experiment. In these calculations no *a priori* consideration was given to the antiferromagnetic state of Cr, nor to the relativsitic effects which should yield small corrections in W. In all three metals the Fermi surfaces were computed in the same manner, using the APW method. These calculations were programmed such that constant-energy surfaces could be traced out in the Brillouin zone. The volumes contained by the various pieces of surface were determined, and the Fermi energy chosen by the requirement of equal hole and electron volumes. A discussion of the methods employed is given in the following sections.

THEORY

Hartree-Fock-Slater Self-Consistent-Field Calculation

The potential was constructed from a superposition of atomic potentials centered on the lattice sites. The atomic potentials were found from Hartree-Fock-Slater (HFS) self-consistent-field calculations similar to those described in detail by Herman and Skillman[11] (HS). Although the program established for these calculations was different in some details from the one published by HS it provided no additional information. This aspect of the project served only as an independent check of their results. Agreement was established for the Cr-group metals out to the fourth figure in all of the eigenvalues.

In performing these calculations, however, it was found to be more convenient to use a logarithmic scale. Because the distance between radial nodes increases rapidly for a given orbital, it is necessary to use an expanding scale of some sort. HS chose to periodically increase the increment size. This can be avoided by using $x=\ln r$ as the independent variable. By simultaneously changing the dependent variable from R to $r^{1/2}R$, we obtain a radial equation containing no first derivative. This has been pointed out by Hartree.[12]

A different method for the numerical integration of the radial equation was used. The method commonly employed is due to Hartree and consists of comparing inward and outward integrations of the radial equation (for a trial eigenvalue) in the region of the outermost inflection point. This technique assures that the solutions have the proper behavior at the two boundaries. The trial eigenvalue is adjusted on the basis of the mismatch in logarithmic derivatives at the joining point. The method for this is developed from perturbation theory and involves an integration over the radial coordinates. A method is presented in the Appendix which eliminates the need for this joining point and hence avoids the problems associated with making the function continuous at this point. In addition, the corrections to the eigenvalue are given by an algebraic expression which can be easily evaluated after each sweep over the range of the radial coordinate.

The result of the HFS calculations is a tabular record of the self-consistent potential and the atomic orbitals with corresponding eigenvalues. In the construction of the muffin-tin potential, the only information needed is the total electronic charge density which one obtains from the orbitals.

The crystal potential was constructed by superposing atomic potentials centered on neighboring lattice sites. In the Slater free-electron approximation the average exchange potential is proportional to $\rho^{1/3}$, where ρ is the total electronic charge density. This requires that the superposing be done in two steps. The ordinary electrostatic potential given by the solution of Poisson's equation, using the charge density ρ, is superposed to give the electrostatic contribution to the crystal potential. The charge density itself is then independently superposed to approximate the crystal charge density. The $\rho^{1/3}$ exchange potential is then computed using this superposed charge density. The resulting contribution is added point by point to the crystal electrostatic potential to yield the total crystal potential.

The method of superposing the radial functions should be discussed. Starting with the function (it might be the electrostatic potential or the charge density) on a particular site, we consider the contributions from the same function centered on neighboring sites. It we limit ourselves to constructing a spherically symmetric potential, then the contributions from neighboring centers will depend only on the distance from the origin to the site. There will, in general, be several equidistant neighbors, and hence these can all be taken into account simultaneously by an appropriate factor.

A procedure for determining the contribution from the function $\chi(r)$ centered on a lattice site a distance R_n from the origin was given by Löwdin[13] and is known as the alpha summation method. This method is very general and allows the construction of a nonspherically symmetric potential. By retaining only the lowest order term in the spherical-harmonic expansion, the resulting expression is simply

$$\chi(r,R_n)=\frac{1}{2rR_n}\int_{|r-Rn|}^{r+Rn} t\chi(t)dt. \qquad (1)$$

This gives the spherically symmetric contribution at r due to the function $\chi(t)$ centered at R_n. Thus the super-

[11] F. Herman and S. Skillman, *Atomic Structure Calculations* (Prentice-Hall, Inc., Englewood Cliffs, New Jersey, 1963).

[12] D. R. Hartree, *Calculation of Atomic Structures* (John Wiley & Sons, Inc., New York, 1957).

[13] P. O. Löwdin, Advan. Phys. **5**, 1 (1956).

position consists of summing these contributions from all the lattice sites in the vicinity of the origin.

The resulting potential, it is hoped, will be slowly varying in the region between atomic sites because of the overlapping of the functions from adjoining neighbors. Of course, it will not be exactly constant; but in many cases it is meaningful to spherically average the potential in this outer region and replace it by a constant value. This was the procedure followed in these calculations. This constant was then subtracted from the spherically-symmetric potential inside the Slater sphere so that the potential in the outer region could be taken as zero. The resulting potential was used in constructing the APW matrix elements as discussed in the following section.

APW Method

The APW method has certainly been established as an important tool in the calculation of electronic properties of crystals. In order to avoid listing the impressive array of theoretical results already produced by this method, only the recent results by Mattheiss[14] will be cited. One can easily trace the abundant literature by starting with this reference. For the most recent results the reader is referred to the Progress Reports of the Solid State and Molecular Theory Group at MIT. All of this work has been motivated by J. C. Slater who was responsible for the original formulation of the method in 1937.[15]

The method takes full advantage of the muffiin-tin form of the potential and constructs a basis function from plane waves and from atomic orbitals in the spherically-symmetric potential. The APW for an electronic state $\bar{k}$ consists of a plane wave in the outer region and a summation of atomic orbitals inside the Slater sphere. The coefficients in the atomic-orbital expansion are chosen such that the functions in each region are continuous on the Slater sphere. The resulting APW, however, has a kink due to a discontinuity in the slope. This is taken into account by including appropriate surface integrals in the matrix elements. These integrals give the contribution to the kinetic energy due to the kink in the wave function. The resulting matrix elements are given here for one atom in the unit cell of volume Ω:

$$(H-E)_{ij}=(\bar{k}_i\cdot\bar{k}_j-E)\left(\delta_{ij}-\frac{4\pi R^2}{\Omega}\frac{j_1(|\bar{k}_j-\bar{k}_i|R)}{|\bar{k}_j-\bar{k}_i|}\right)$$
$$+\frac{4\pi R^2}{\Omega}\sum_{l=0}^{\infty}(2l+1)P_l(\hat{k}_i\cdot\hat{k}_j)j_l(k_iR)$$
$$\times j_l(k_jR)[\mu_l'(R,E)/\mu_l(R,E)]; \quad (2)$$

R is the radius of the Slater sphere and can be any value (less than half of the interatomic spacing) such that the potential in the region outside the sphere is nearly constant. The radii used in this calculation are listed in Table I. The l summation was truncated at $l=10$. The Legendre polynominals $P_l(Z)$ were calculated from the recurrence relation

$$lP_l(Z)=(2l-1)ZP_{l-1}(Z)-(l-1)P_{l-2}(Z), \quad (l\geq 2) \quad (3)$$

starting with $P_0(Z)=1$ and $P_1(Z)=Z$. The spherical Bessel functions were computed from the recurrence relation

$$j_l(Z)=\frac{2(l-\frac{1}{2})}{Z}j_{l-1}(Z)-j_{l-2}(Z). \quad (4)$$

The standard method for calculating these functions is to start with two arbitrary values $j_L(Z)$ and $j_{L-1}(Z)$ where L is large enough that $j_L(Z)$ is in the asymptotic region. After determining the functions $j_l(Z)$ from $l=L$ down to $l=0$ with the recurrence relation, the normalization can be fixed by computing any of the lower order functions explicitly. This method avoids the loss in accuracy resulting from repeatedly subtracting numbers which are almost equal. Finally, the logarithmic derivatives of the radial functions can be determined from outward integrations of the radial equation, using finite-difference approximations similar to those described in Appendix A.

The secular determinant resulting from the linear variation function using APW's gives the dispersion relation $E(\bar{k})$ for the conduction electrons. It should be noticed that the energy appears both explicitly and implicitly in these matrix elements. Hence the eigenvalue problem necessarily involves finding the roots of the secular equation numerically. Having specified the quantum numbers of the crystalline state $(\bar{k})$, it is necessary to examine the determinant as a function of energy and find the roots. For a given value of energy it is necessary to perform an outward integration of the radial equation for each value of l. This requires extensive computing, and so in this work it was decided to fix the energy parameter and solve the resulting eigenvalue problem for the constant-energy surfaces. In this way the integrations could be performed once and for all, and only the algebra associated with the other terms in the matrix elements had to be repeated each time. This does not represent a great saving of computer time, but it does yield important information

TABLE I. Some parameters and results of APW calculation.

	Cr	Mo	W
Lattice constant	5.4512	5.9468	5.9810
Slater-sphere radius	2.34	2.46	2.46
Fermi energy	0.647	0.542	0.548
Density of states $G(E)$	0.0895	0.0695	0.0673
Electronic-specific-heat coefficient (cal/mole°K²)	3.00(−4)	3.04(−4)	2.98(−4)

[14] L. F. Mattheiss, Phys. Rev. **134**, A970 (1964).
[15] J. C. Slater, Phys. Rev. **51**, 846 (1937).

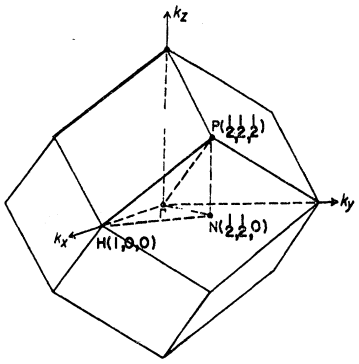

FIG. 1. Brillouin zone for body-centered cubic-crystal lattice.

about the energy surfaces near the Fermi surface. Of course one does not know the Fermi energy *a priori*. However, the requirement that electron and hole volumes be equal is sufficient to determine the Fermi energy. This aspect of the calculations will be discussed in more detail later in the paper. It might be mentioned for the sake of completeness that the secular determinants were solved by the method of triangularzation. This amounts to getting zeros under the main diagonal by adding and subtracting multiples of the rows. A few systematic attempts at this will lead one to the expression

$$D_{\mu\nu}=d_{\mu\nu}-\sum_{i=1}^{I-1}\frac{D_{\mu i}D_{i\nu}}{D_{ii}} \tag{5}$$

where I is the minimum value of ν or μ. This gives the rule for transforming the original matrix elements $d_{\mu\nu}$ into the triangularized form. The value of the determinant is then πD_{ii}.

Lattices

The crystal structure for the chromium group metals is bodycentered cubic. The lattice constants[16] are listed in Table I.[17] This structure and the associated

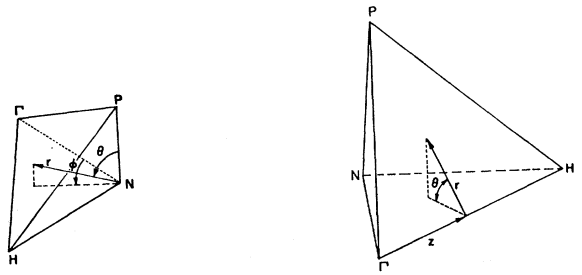

FIG. 2. 1/48 zone showing coordinate systems used in tracing energy contours.

[16] *International Tables for X-ray Crystallography* (Kynoch Press, Birmingham, England, 1962), Vol. III.

[17] Units are such that $e^2=2$, $m=\frac{1}{2}$ and $h=2\pi$. Thus energies are in rydbergs and distances in Borh radii.

reciprocal lattice are reviewed by Jones.[18] The Brillouin zone is shown in Fig. 1. The 1/48 zone is outlined by the points of high symmetry ΓPNH. The coordinates of these points are indicated on the figure in units of $2\pi/d$. In this calculation the set of 19 reciprocal lattice vectors nearest the origin were used for all points throughout the zone. This is a slight disadvantage to the points near the P, N, and H. By increasing the basis set to 26 lattice vectors, one can include all those vectors for which $|\bar{k}+\bar{K}|\leq 4\pi/d$ with $\bar{k}$ anywhere in the 1/48 zone. This probably would have been better, but the calculations were much too extensive to repeat for this reason alone.

In the Lomer model the Fermi surface is located along the ΓH axis and at the point N. Anticipating this, two coordinate systems for tracing out the energy contours were established: cylindrical coordinates with ΓH as the azimuthal axis and angles measured from the ΓNH, and spherical coordinates centered at N with NP as the azimuthal axis and angles measured from the plane $N\Gamma P$. These coordinate systems in the 1/48 zone are shown in Fig. 2.

Constant-Energy Contours

The procedure for tracing out the constant-energy surfaces will be discussed. Along ΓH for instance, the polar angle between the planes ΓPH and ΓNH was divided into four equal intervals. Then for a particular plane the z coordinate was specified, and the secular determinant was examined as a function of the radial coordinate to determine the roots. These roots were located by searching for a change of sign and then using repeated linear interpolations. The roots represent the intersection of the energy surface with the plane. A similar procedure was carried out at the symmetry point N where the azimuthal angle between the planes $NP\Gamma$ and $N\Gamma H$ was also divided into four intervals.

RESULTS AND DISCUSSION

Fermi Energy and Density of States

The volume contained by each of the pieces of surface for a particular value of the energy were numerically determined from the tabular data. The assignment of electrons and holes to the various regions was determined on the basis of whether the volume increased or decreased with an increase in the energy. In Fig. 3 these volumes are plotted as a function of the energy for the three metals. The Fermi energy is determined by the requirement of equal hole and electron volumes. The results are given in Table I.

The density of states at the Fermi energy can be determined from Fig. 3. The definition of the density of

[18] H. Jones, *The Theory of Brillouin Zones and Electronic States in Crystals* (Interscience Publishers, Inc., New York, 1960).

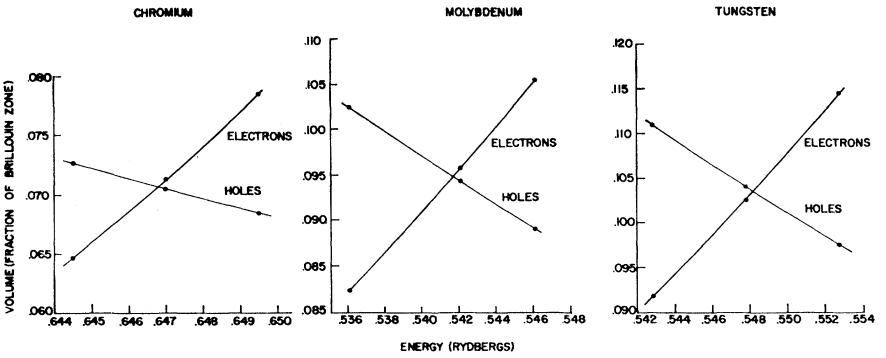

FIG. 3. Hole and electron volumes contained by energy surfaces.

states is

$$G(E)=(1/4\pi^3)dV_k/dE, \quad (6)$$

where $G(E)dE$ is the number of electrons per unit volume of the crystal (the factor of 2 for spin degeneracy is already included) with energy in the range E to $E+dE$. dV_k is the volume in reciprocal space between the constant energy surfaces E and $E+dE$. dV_k/dE is therefore the slope of the volume-versus-energy curve. Thus

$$dV_k/dE=48[(dv_e/dE)-(dv_h/dE)]. \quad (7)$$

The v corresponds to volume in the 1/48 zone; subscripts refer to electrons and holes. The minus sign is needed because an increase in energy results in a decrease in the hole volume. The values of $G(E)$ determined from Fig. 3 are given in Table I. The low-temperature electronic-specific-heat coefficient is related to this by

$$\gamma=(\pi^2/3)(k^2/\rho)G(E), \quad (8)$$

where k is the Boltzmann constant and ρ is molar density. The predicted specific-heat coefficients are listed in Table I.

Fermi Surfaces

The energy surfaces calculated for the middle set of points in each of the curves in Fig. 3 are shown in Figs. 4, 5, and 6. One notices immediately that the surfaces for Mo and W are quite similar and exhibit the qualitative features of the Lomer model (see Fig. 7). Cr differs from these by the absence of the hole pockets at N and by a reduction in the size of the knobs on the electron jack. The pockets along ΓH are found to contain electrons. A quantitative comparison between these surfaces and experimental results will now be considered. Because Cr is complicated by the magnetic state and W is heavy enough for relativistic effects to be important, the characteristics of the Fermi surface of Mo will be emphasized.

The de Haas–van Alphen frequencies can be predicted from extremal areas of the Fermi surface using the Onsager relation $f=KA_0$ where $K=c\hbar/2\pi e=374.1(6)$. This gives f in G with A_0 measured in atomic units. The various extremal orbits are shown in Figs. 8 and 9. The corresponding de Haas–van Alphen frequencies

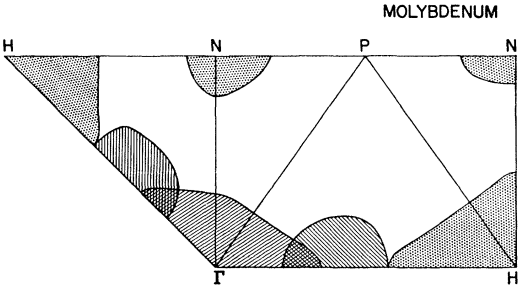

FIG. 5. Intersection of molybdenum Fermi surface with 1/48 zone faces.

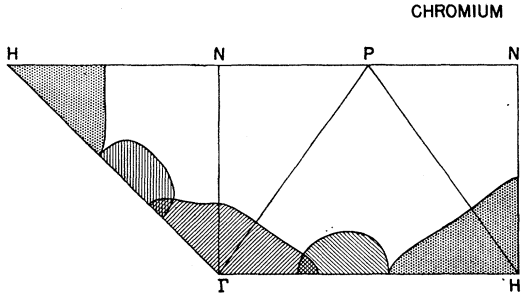

FIG. 4. Intersection of chromium Fermi surface with 1/48 zone faces.

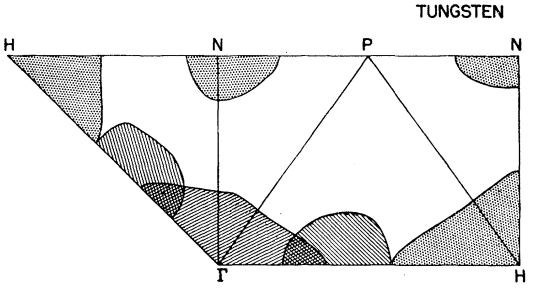

FIG. 6. Intersection of tungsten Fermi surface with 1/48 zone faces.

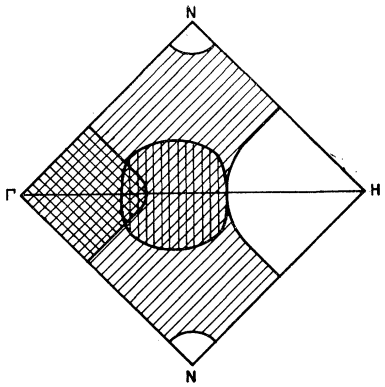

FIG. 7. Lomer model for chromium-group metals.

are listed in Table II. Without detailed angular dependence of these frequencies it is difficult to compare all of them with experiment. For instance, the holes at N and the electron pockets along ΓH should have complicated angular dependence because of the different possible orientations of each in the Brillouin zone. There are the equivalent of 6 hole pockets and 6 electron pockets in the first zone (Fig. 1). However, Brandt and Rayne[6] have reported a large number of frequencies for Mo ranging from 5.03 to 8.00(6) G. Most of these can apparently be associated with the small electron pockets along ΓH. The larger frequencies reported approach the magnitude predicted for the $J_1(100)$ orbit around the necks of the jack. They also report two frequencies at 24.2 and 25.8(6) G for the (110) direction. These fall in the range of frequencies predicted for the holes at N. In fact, the extremal area of the hole pockets in the plane NPH [which corresponds to one of the (110) frequencies] yields the frequency 24.1(6) G. For completeness, the $NP\Gamma$ cross section yields 30.6(6) and ΓNH yields 16.5(6) G.

A further comparison can be made with the de

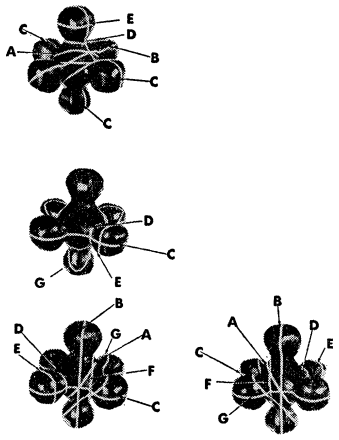

FIG. 8. Orbits on molybdenum electron jack. (A)-J_1 (111); (B)-J_1(110) (C)-J_1(100); (D)-J_2(100), (E)-J_3(100); (F)-J_4(110); (G)-J_5(111).

Haas–van Alphen measurements on Mo communicated by Girvan.[19] In the (111) direction he has preliminary results which indicate frequencies at 5.7, 25.5, 31.6, 37.2, 91 and 110(6) G. The first of these could be assigned to the electron pockets along ΓH. The next three are in the range predicted for the holes at N. Of course, the frequencies from orbits on the knobs of the jack (orbit J_3) are expected to be about 35(6) G. Thus, the higher frequencies from the holes at N and the ones from the knobs are the of same magnitude. Considering the two larger frequencies, the value 91(6) G could be associated with either the orbit $J_1(111)$ or $J_5(111)$. The latter was not determined exactly, but is probably a little larger than $J_1(111)$ which yields a frequency of 72.3(6) G. The experimental value 110(6) G agrees closely with the theoretical value for the hole orbit $H(111)$.

Girvan also reports the following possible frequencies in the (100) direction: 5.43, 10.8, 24.0, 33.3, and 165(6) G. The smallest value is gain attributed to the elec-

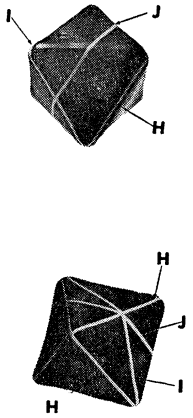

FIG. 9. Orbits on molybdenum hole octahedron. H-$H(100)$; I-$H(110)$; J-$H(111)$.

tron pockets along ΓH. The next frequency 10.8(6) G is either a harmonic or might be associated with the neck orbit $J_2(100)$. The intermediate values are of the same order of magnitude as the predicted frequencies for the holes at N or for the knob orbit $J_3(100)$. The largest frequency agrees closely with the predicted value 168(6) G for the holes at H.

From the above discussion it is concluded that the large orbits on the electron jack and the hole octahedron are easily identified and agree quantitatively with the experimental results of Girvan. Also it is likely that the smaller frequencies reported by Brandt and Rayne are due to orbits on the electron pockets along ΓH. The frequencies of the orbits on the hole pockets at N range from about 16 to 32(6) G, but the frequencies from the knobs on the jack should overlap the upper portion of this range. Only the availability of the

[19] R. F. Girvan (private communication). I am grateful to Mr. Girvan for informing me of these results prior to publication.

TABLE II. Predicted de Haas–van Alphen frequencies (G).

	Orbit	Frequency
Electron jack		
	$J_1(100)$	227. $\times 10^6$
	$J_2(100)$	11.3
	$J_3(100)$	33.6
	$J_1(110)$	154.
	$J_4(110)$	64.7 → 76.4
	$J_1(111)$	72.3
	$J_5(111)$	Not measured
Hole octahedron		
	$H(111)$	108
	$H(110)$	130
	$H(100)$	168
Holes at N		
	All directions	16.5 → 32.3
Electron pockets ΓH		
	Not calculated—Same order of magnitude as $J_2(100)$.	

experimentally determined angular dependence of the frequencies would clarify this assignment of orbits.

The size-effect data of Walsh *et al.*,[20] on W provide a further comparison with the theoretical results. The extremal dimensions of the jack and the octahedron are listed in Table III.[21] Since Mo and W have essentially the same Fermi surfaces if relativistic effects are neglected, one can presumably see from this table the changes in the surface caused by these effects. As Walsh[10] has pointed out, the jack and octahedron must be split apart along ΓH by the spin-orbit coupling.

Another experimental result which can be predicted is the low temperature electronic-specific-heat coefficient γ. This was discussed in a previous section of the paper.

TABLE III. k vectors of Fermi surface.

	W (expt)[a]	W (theory)[b]	Mo (hteory)[c]
Electron jack			
(100)	0.587	0.613	0.608
(110)	···	0.270	0.257
(111)	0.219	0.248	0.232
Hole octahedron			
(100)	0.411	0.428	0.445
(110)	0.316	0.317	0.332
(111)	0.265	0.264	0.282
Holes at N			
along NP	···	···	0.195
along $N\Gamma$	···	···	0.141
along ΓH	···	···	0.100

[a] Walsh *et al.*
[b] Matheiss (Ref. 21) APW calculation.
[c] Present work.

[20] W. M. Walsh, Jr., and C. C. Grimes, Phys. Rev. Letters **13**, 523 (1964).
[21] L. F. Mattheiss and R. E. Watson, Phys. Rev. Letters **13**, 526 (1964).

TABLE IV. Electron specific heat coefficient $\gamma(10^{-4}$ cal/mole°K$^2)$.

	Cr	Mo	W
Present work	3.00	3.04	2.98
Manning and Chodorow (Ref. 4)	···	···	4.8
Horowitz and Daunt (Ref. 22)	···	5.1 ±0.4	1.8 ±0.7
Gupta, Cheng, and Beck (Ref. 23)	3.76	···	···
White and Woods (Ref. 24)	3.60	5.24	2.88
Kirillin, Sheindlin, and Chekhovskoi (Ref. 25)	···	···	10.1
Shimizu, Takahashi, and Katsuki (Ref. 26)	3.7 –3.8	5.05–5.25	1.8 –5.0
Clusius and Franzosini (Ref. 27)	3.6	···	···

The theoretical values are presented in Table IV with a variety of experimental results.[22–27]

As a final comparison with experiment, those properties which depend on the surface area of the Fermi surface were predicted for Mo. The surface area of the jack was determined in a rather crude fashion. Therefore all values are quoted to only two significant figures. The results are given in Table V. Fawcett and Griffiths[28] have experimentally examined the anomalous skin effect for the Cr-group metals. The quantity measured is $\langle 1/\Sigma \rangle$ where Σ is the surface conductance. By using $\langle 1/\Sigma \rangle^{-3}$ for $\langle \Sigma^3 \rangle$ they were able to calculate the surface area S using

$$S = (6\sqrt{3}\pi^2\omega^2 h/e^2)\langle \Sigma \rangle^3. \quad (9)$$

The above approximation in the averaging procedure is known to underestimate S for anisotropic surfaces. The experimentally determined value for Mo is 1.74 a.u. as compared to our value of 6.7 a.u. Using the

TABLE V. Surface area of Mo and related parameters.

Electron jack	3.2
Hole octahedron	1.6
Electron pockets (6)	0.4
Holes at N (6)	1.5
	—
Total surface area	6.7 atomic units (a. u.)
$\langle 1/v \rangle^{-1}$	7.6×10^7 cm/sec
$\sigma/\langle l \rangle$	7.4×10^{14} esu

[22] M. Horowitz and J. G. Daunt, Phys. Rev. **91**, 1099 (1953).
[23] K. P. Gupta, C. H. Cheng, and P. A. Beck, J. Phys. Radium **23**, 721 (1962).
[24] G. K. White and S. B. Woods, Phil. Trans. Roy. Soc. London **215A**, 35 (1959).
[25] V. A. Kirillin, A. E. Sheindlin and V. Ya. Chekhovskoi, Chem. Abstr. **57**, 1632 F (1962).
[26] M. Shimizu, T. Takahashi and A. Katsuki, J. Phys. Soc. Japan **17**, 1740 (1962).
[27] K. Clusius and P. Franzosini, Gazz. Chim. Ital. **93**, 221 (1963).
[28] E. Fawcett and D. Griffiths, J. Phys. Chem. Solids **23**, 1631 (1962).

theoretical values for S and γ, two additional physical quantities can be calculated[29]:

$$\sigma/\langle l\rangle=(e^2S)/(6\pi^2h), \tag{10}$$

$$\langle 1/v\rangle=(6h\gamma)/(k^2S). \tag{11}$$

σ is the dc conductivity, $\langle l\rangle$ is the electron mean free path, and v is the electron velocity at the Fermi surface. These results are also listed in Table V although they are not readily compared with experiment.

APPENDIX

An algorithm for the numerical of the radial Schrödinger equation is discussed in this Appendix. This equation takes the form

$$Y''(x)=g(x)Y(x) \tag{A1}$$

where $Y=r^{1/2}R$ and $x=\ln r$. Here

$$g(x)=e^{2x}[\lambda+V(e^x)]+(l+\tfrac{1}{2})^2 \tag{A2}$$

with $\lambda=-E$. By writing the Taylor series expansion at r, it is easy to show that

$$Y_{j+1}-2Y_j+Y_{j-1}=\Delta^2Y_j''+(\Delta^4/12)Y_j^{iv}. \tag{A3}$$

Differentiating this twice and dropping the highest order term, the fourth derivative can be expressed in terms of second derivatives at neighboring points. Using the original differential equation to eliminate the second derivative we find

$$A_jY_{j+1}+B_jY_j+C_jY_{j-1}=0, \tag{A4}$$

where

$$\begin{aligned} A_j&=1-(\Delta^2/12)G_{j+1},\\ B_j&=-2-(5\Delta^2/12)G_j,\\ C_j&=1-(\Delta^2/12)G_{j-1}. \end{aligned} \tag{A5}$$

The differential equation is thus replaced by a tridiagonal system of linear equations with coefficients which depend on the eigenvalue and the potential. We approach the solution of this set of equations by taking

$$\begin{aligned} \lambda+\lambda\delta&=\lambda^*,\\ Y_j+\delta Y_j&=Y_j^*. \end{aligned} \tag{A6}$$

The philosophy is to assume that the true solution λ and Y_j differ from a trial solution (indicated by a star) only by the small quantities $\delta\lambda$ and δY_j. This necessitates a reasonable initial guess for the wave function and eigenvalue. Since in general λ^* and Y_j^* will not satisfy the difference equation, we write

$$A_jY_{j+1}^*+B_jY_j^*+C_jY_{j-1}^*=Q_j. \tag{A7}$$

[29] A. B. Pippard, Rept. Progr. Phys. **23**, 176 (1960).

Q_j is called the residual; it will approach zero as λ^* and Y_j^* approach the correct solution. Using (A5) and (A6) it is not difficult to show that (A7) becomes

$$A_j\delta Y_{j+1}+B_j\delta Y_j+C_j\delta Y_{j-1}+D_j\delta\lambda=Q_j, \tag{A8}$$

where

$$D_j=-(\Delta^2/12)e^{2x}(e^{2\Delta}Y_{j+1}^*+10Y_j^*+e^{-2\Delta}Y_{j-1}^*). \tag{A9}$$

We assume a solution in the form

$$\delta Y_j=E_j\delta Y_{j+1}+F_j\delta\lambda+G_j. \tag{A10}$$

Repeated substitution into (A8) yields

$$\begin{aligned} E_j&=-A_j/R_j,\\ F_j&=-(D_j+C_jF_{j-1})/R_j,\\ G_j&=(Q_j-C_jG_{j-1})/R_j, \end{aligned} \tag{A11}$$

with

$$R_j=B_j+C_jE_{j-1}. \tag{A12}$$

The solution at each stage of the iteration then follows after the boundary conditions are specified. The inner boundary condition at $x\to-\infty$ allows us to set

$$E_1=e^{\Delta/2},\quad F_1=0\quad\text{and}\quad G_1=Y_1^*-E_1Y_2^*. \tag{A13}$$

From repeated application of (A11) we can then determine E_J,F_J and G_J corresponding to a grid point in the outer tail region of the wave function. In this region the WKB approximation is valid, and it is not difficult to show from a comparison of (A10) and the asymptotic form of the wave function that

$$\delta\lambda=(Y_{J-1}^*-G_{J-1}-a_J)/(F_{J-1}-b_Ja_J), \tag{A14}$$

where

$$\begin{aligned} a_J&=Y_J^*\exp(\Delta\sqrt{g_J}),\\ b_J&=\Delta\exp(-2x_J)/(2\sqrt{g_J}). \end{aligned}$$

Here J corresponds to the grid point at the outer boundary and x_J is the value of x at that point. Having determined $\delta\lambda$ from (A14), we set $\delta Y_J=0$ in order to specify the normalization. Then repeated application of (A10) yields the corrections to the trial wave function.

This algorithm has been found to converge after only a few iterations in most instances. However, it is usually necessary to do some preliminary calculations before using this method. It should be obvious that the trial function must have the same number of nodes desired for a particular orbital. Hence, the same procedure suggested by Hartree and used by HS for counting nodes and getting an approximate eigenfunction and eigenvalue is recommended. This is particularly important for the higher orbitals where the eigenvalues get very close together.